DoReMi: A Domain-Representation Mixture Framework for Generalizable 3D Understanding

Mingwei Xing* Xinliang Wang* Yifeng Shi[†] Ke Holdings Inc.

{xingmingwei001, wangxinliang008, shiyifeng003}@ke.com

Abstract

The generalization of 3D deep learning across multiple domains remains limited by the limited scale of existing datasets and the high heterogeneity of multi-source point clouds. Point clouds collected from different sensors (e.g., LiDAR scans and mesh-derived point clouds) exhibit substantial discrepancies in density and noise distribution, resulting in negative transfer during multi-domain fusion. Most existing approaches focus exclusively on either domain-aware or domain-general features, thereby overlooking the potential synergy between them. To address this, we propose DoReMi (Domain-Representation Mixture), a Mixture-of-Experts (MoE) framework for generalizable 3D understanding. It integrates a **Domain**-aware Experts branch and a unified Representation branch to enable cooperative learning between specialized and generalizable knowledge. DoReMi dynamically activates domain-aware expert branch via Domain-Guided Spatial Routing (DSR) for context-aware expert selection and employs Entropy-Controlled Dynamic Allocation (EDA) for stable and efficient expert utilization, thereby adaptively modeling diverse domain distributions. Complemented by a frozen unified representation branch pretrained through robust multiattribute self-supervised learning, DoReMi preserves crossdomain geometric and structural priors while maintaining global consistency. We evaluate DoReMi across multiple 3D understanding benchmarks. Notably, DoReMi achieves 80.1% mIoU on ScanNet Val and 77.2% mIoU on S3DIS, demonstrating competitive or superior performance compared to existing approaches, and showing strong potential as a foundation framework for future 3D understanding research. The code will be released soon.

1. Introduction

In recent years, with the advancement of deep learning models [10, 14, 50, 60] and the continuous release of di-

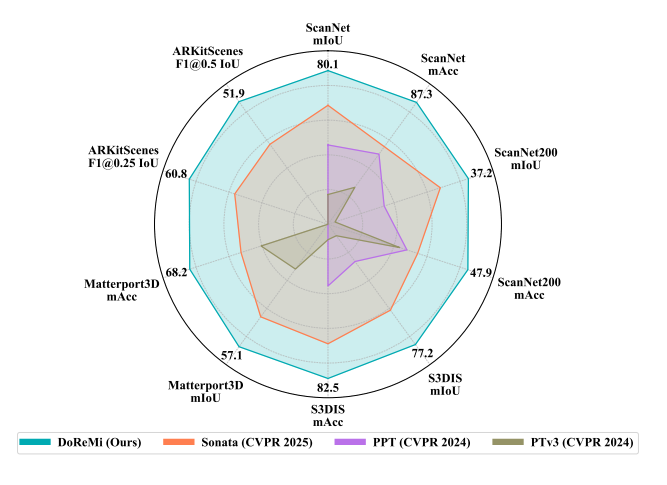


Figure 1. **Performance of DoReMi**. DoReMi advances multiple state-of-the-art benchmarks on 3D scene understanding datasets.

verse 3D datasets [2, 8, 55], 3D deep learning has achieved remarkable progress in tasks such as semantic segmentation, object detection, and other 3D understanding applications [6, 23, 48]. However, compared with 2D vision tasks, the 3D vision field still faces the dual challenges of limited dataset scale and high cross-domain heterogeneity. On one hand, 3D data acquisition and annotation are costly, resulting in far fewer large-scale labeled datasets than in 2D vision (e.g., ImageNet [9], Objects365 [38], LION [37]). On the other hand, significant discrepancies exist between point clouds obtained from different acquisition or generation methods—for example, sparse point clouds from LiDAR scanning versus dense point clouds sampled from multi-view reconstruction or mesh surfaces—exhibiting pronounced differences in point density, noise patterns, and geometric details, which substantially limits cross-domain generalization.

To address these challenges, prior studies fall into two main directions. The first focuses on domain-aware feature learning, using customized architectures [21], feature modulation [32], or domain-specific losses [54] to enhance representation within specific domains. The second emphasizes unified representation learning, extracting shared geo-

^{*}Equal contribution † Corresponding author

metric and structural priors [27, 49, 51] for improved generalization across domains. However, these two directions are usually studied separately, overlooking their complementarity: domain-aware features capture fine-grained, adaptive information, while unified representations preserve transferable global semantic structures. How to jointly model and exploit both types of features within a unified framework remains an open and important research problem.

Thus, we propose DoReMi (Domain-Representation Mixture), a Mixture-of-Experts (MoE) framework that jointly models domain-aware and unified representation features, enabling complementary learning of cross-domain and intra-domain knowledge. The Domain-aware branch (Do) employs Domain-Guided Spatial Routing (DSR) for context-aware expert selection and Entropy-Controlled Dynamic Allocation (EDA) for stable and efficient expert allocation, allowing adaptive modeling of diverse domain distributions. In parallel, DoReMi incorporates a frozen unified Representation branch (Re) pretrained via robust multiattribute self-supervised learning, which preserves crossdomain geometric and structural priors to ensure robust global generalization. As shown in Figure 1, DoReMi achieves superior performance compared to previous stateof-the-art methods across multiple 3D understanding tasks. Our main contributions are summarized as follows:

- Integrated DoReMi framework. We propose DoReMi, an integrated Mixture-of-Experts framework that jointly models domain-aware and general features, enabling complementary learning between domain-specific adaptability and cross-domain generalization.
- Joint learning of domain-aware and unified representations. DoReMi incorporates three components to enable effective collaboration between the domain-aware and unified representation branches: DSR for contextaware expert selection, EDA for stable and efficient expert allocation, and Re branch pretrained via robust multi-attribute self-supervision to retain cross-domain geometric and structural priors. Together, these designs enable adaptive domain modeling with semantic consistency.
- Comprehensive evaluation and SOTA performance. Extensive experiments on multiple indoor and outdoor 3D understanding benchmarks demonstrate that DoReMi consistently outperforms existing approaches, achieving 80.1% mIoU on ScanNet Val and 77.2% mIoU on S3DIS, further advancing the state of the art in 3D understanding. Our framework can be further enhanced through integration with advanced pretraining strategies.

2. Related Work

2.1. 3D Understanding

3D scene understanding is a fundamental problem in computer vision, encompassing a variety of downstream tasks

such as semantic segmentation [29–31, 43, 51], object detection [19, 39, 63], and instance segmentation [15, 18]. Early methods mainly relied on hand-crafted geometric features or voxel-based representations, which suffered from discretization artifacts and limited scalability. With the advancement of deep learning, point-based [30, 43] and transformer-based [45, 47] architectures have achieved significant performance gains by directly operating on irregular point sets or exploiting attention-based contextual mod-Despite this progress, most existing 3D understanding models are tailored for specific datasets or sensor modalities, lacking robust generalization across diverse domains. In this context, our proposed DoReMi framework can serve as a universal 3D feature extractor, capable of providing both domain-adaptive and cross-domain generalizable representations, thereby enhancing the performance of various downstream 3D understanding tasks.

2.2. Adaptive and Unified 3D Representation Learning

Learning unified and adaptable 3D representations across diverse domains and modalities has attracted increasing attention. Existing studies mainly pursue two complementary directions. Domain-aware feature learning enhances adaptability through customized architectures, feature modulation, or domain-specific objectives, as seen in adaptive normalization [21], multi-scale alignment [32], and geometry alignment [54]. These methods achieve strong domainspecific representations but often lack cross-domain generalization. Conversely, unified representation learning focuses on extracting shared geometric and structural priors to improve generalization and robustness, with representative works including contrastive or self-supervised learning [27, 31, 51, 57], multimodal alignment [28, 52], and large-scale 3D foundation models [49, 62]. In contrast, DoReMi integrates these two perspectives within a MoE framework, jointly capturing domain-aware adaptability and representation-level generalization for balanced and robust 3D understanding.

2.3. Mixture-of Experts

The Mixture-of-Experts (MoE) paradigm [17, 34] has recently attracted growing attention in both natural language processing and computer vision due to its ability to improve model capacity and specialization efficiency. In the vision domain, MoE has been applied to image classification [35], visual transformers [11, 13], and multimodal representation learning [24], enabling conditional computation and task-specific feature routing. More recently, several studies have explored MoE designs in 3D understanding [22, 58], focusing mainly on efficiency improvement or model scaling. Unlike these approaches, DoReMi integrates domain-aware and representation-general branches to encourage comple-

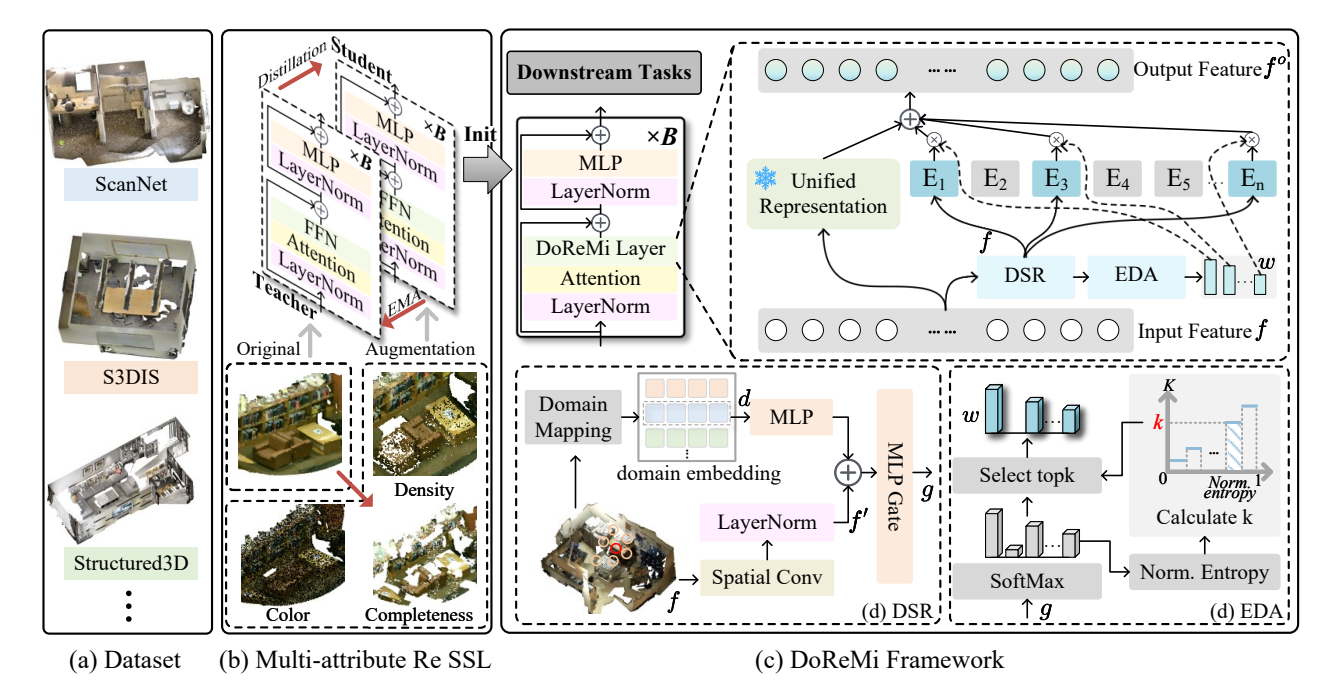


Figure 2. The architecture of DoReMi. It combines two branches: a domain-aware branch (Do) and a unified-representation branch (Re). DoReMi starts with a pretrained model generated through self-supervised learning on multi-attribute data. Re freezes this pretrained knowledge to extract cross-domain geometric and structural patterns. Meanwhile, Do uses Domain-Guided Spatial Routing (DSR) and Entropy-Controlled Dynamic Allocation (EDA) to capture domain-specific features. Together, these branches enhance both domain adaptability and generalization.

mentary learning and employs DSR and EDA to achieve stable and interpretable expert selection.

3. Method

3.1. Overview

We propose DoReMi (Domain–Representation Mixture), a Mixture-of-Experts (MoE) architecture designed for generalizable 3D understanding. DoReMi jointly models domain-aware expert features and unified representation features, enabling adaptive modeling of diverse domain distributions while maintaining cross-domain consistency and generalization capability. The overall architecture is illustrated in Figure 2. Specifically, we first employ a teacherstudent network framework [41] to conduct multi-attribute self-supervised learning across multiple datasets, thereby learning geometric domain-structure priors that generalize across domains. Subsequently, the DoReMi architecture undergoes multi-domain supervised joint training, with its weights initialized from the student network. FFN weights are duplicated for both the Re and Do branches, while the Re branch remains frozen. Do branch consists of two components: Domain-Guided Spatial Routing (DSR) and Entropy-Controlled Dynamic Allocation (EDA). DSR performs expert selection by leveraging learnable domain embeddings and spatial context awareness, while EDA

achieves robust and adaptive expert assignment by computing the uncertainty of the routing outputs.

3.2. Unified Representation Branch

We introduce a frozen Unified Representation branch (Re), which is constructed through large-scale multi-attribute self-supervised learning. This branch aims to capture geometric structures, spatial layouts, and semantic priors shared across domains. Through systematic comparison of point cloud data across different domains, we observe significant distributional discrepancies, primarily manifested in color distribution patterns, variations in point cloud spatial density, and object incompleteness caused by occlusions and camera viewpoint limitations. These differences lead to a notable degradation in model generalization performance on cross-domain data.

After the above analysis, we design three self-supervised alignment tasks tailored to color, density, and completeness, respectively. Specifically, we partition the point cloud into multiple patches. Within each patch, points are randomly assigned black coloration at varying ratios and probabilities, while certain points are also randomly discarded. Additionally, we apply masking operations to entire patches to simulate variations in point cloud completeness. Inspired by DINOv2 [26] and Sonata [49], we adopt a feature distillation framework based on a teacher-student net-

work architecture, where the teacher's weights are updated via an exponential moving average (EMA) of the student's weights. The teacher receives raw data, while the student receives augmented data. The student is trained to synchronize with teacher through a cluster-based loss [4, 36], ensuring uniform feature consistency across diverse augmentations of the same point cloud. This approach effectively suppresses domain-specific noise, thereby providing stable and robust foundational features for domain-specific experts. Furthermore, we initialize the DoReMi architecture with the weights of the student network, duplicating its FFN for all experts in both Re and Do branches, while keeping Re branch frozen. Given point-level tokens $f \in \mathbb{R}^{N \times D}$, where N denotes the number of tokens and N denotes the feature dimension. The output of Re branch is:

$$f^{\text{Re}} = E_{Re}(f), \tag{1}$$

where E_{Re} denotes the expert in the Re branch.

3.3. Domain-Guided Spatial Routing

To achieve domain-aware expert selection, we design DSR. Given f and its corresponding domain embedding d, we first reshape f into a 3D sparse tensor to capture its local topological structure and positional correlations in the spatial dimensions, and then apply a 3D spatial convolution operation for feature extraction. Through a set of learnable convolutional kernels and normalization, the model effectively extracts feature representations f' with spatial locality awareness. Subsequently, we map the current scene to the corresponding domain embedding d based on its dataset affiliation, and a lightweight MLP then transforms d into a continuous vector $\mathbf{e}_d \in \mathbb{R}^D$ for channel alignment, which encodes domain-specific semantic priors. We add e_d to the spatially convolved feature f' via broadcasting to generate the domain-aware routing input:

$$z = f' + e_d, (2)$$

where $z \in \mathbb{R}^{N \times D}$. This fusion operation ensures that routing decisions depend not only on the input content but are also explicitly guided by the semantic information of the target domain, thereby enhancing the domain adaptability of expert assignment.

The resulting z is then fed into a gating network \mathcal{G} , composed of a MLP with nonlinear activation functions. \mathcal{G} outputs routing logits:

$$g = \mathcal{G}(z) \in \mathbb{R}^{N \times K},\tag{3}$$

where K is the number of experts.

3.4. Entropy-Controlled Dynamic Allocation

Traditional MoE mechanisms fix the number of experts activated per token to a fixed constant, which can lead

to over-computation for simple samples or insufficient expression for complex ones. To address this, we propose EDA. First, we apply softmax function to the gating outputs in last dimension to obtain a probability distribution $p = \operatorname{SoftMax}(g) \in \mathbb{R}^{N \times K}$, and calculate the Shannon entropy for each token:

$$H = -\sum_{j=1}^{K} p[:,j] \odot \log p[:,j], \tag{4}$$

where \odot denotes element-wise multiplication and $H \in \mathbb{R}^N$ reflects the model's decision-making uncertainty for that token. Next, we linearly map the entropy values to the number of experts k to dynamically determine the number of activated experts:

$$k = \left[k_{\min} + \frac{H}{H_{\max}} \cdot (k_{\max} - k_{\min}) \right], \tag{5}$$

where $k \in \mathbb{R}^N$ represents the number of selected experts, $H_{\max} = \log K$ represents the theoretical maximum entropy, with $k_{\min} = 1$ and $k_{\max} = K$, and $\lceil \cdot \rceil$ denotes the ceiling function. Tokens with higher entropy (uncertainty) activate more experts to enhance representation capacity, whereas low-entropy tokens activate fewer experts to improve computational efficiency. We sort the experts in descending order of their probabilities p, and activate the top-k experts with the highest probabilities. Each expert's weight assignment is given by:

$$w[i,j] = \begin{cases} p[i,j], & j \in E_i^{\text{act}} \\ 0, & otherwise, \end{cases}$$
 (6)

where E_i^{act} denotes the indices of the activated experts for i-th token and $w \in \mathbb{R}^{N \times K}$.

To prevent uneven expert load distribution, we adopt a load balancing loss [11]:

$$\mathcal{L}_{\text{balance}} = K \cdot \sum_{j=1}^{K} c_j \cdot r_j,$$

$$c_j = \frac{1}{N} \sum_{i=1}^{N} \mathbb{1}\{j \in E_i^{act}\}, r_j = \frac{1}{N} \sum_{i=1}^{N} p[i, j],$$

$$(7)$$

where c_j is the proportion of tokens routed to expert j, and r_j is the average probability assigned by DSR via softmax function. This loss promotes uniform routing, fostering collaborative learning across all experts.

Finally, after selecting the top-k experts based on the routing probabilities, the output of the Do branch is computed as a weighted sum of the selected experts' outputs.

$$f^{\text{Do}} = \sum_{j=1}^{K} w[:,j] \odot E_j(f).$$
 (8)

Table 1. Indoor semantic segmentation.

Method	Source	ScanNet Val		ScanNet200 Val		S3DIS Area 5				
1/1041/04	Source	mIoU	mAcc	allAcc	mIoU	mAcc	allAcc	mIoU	mAcc	allAcc
SparseUNet [7]	CVPR 2019	72.3	80.2	90.0	25.0	32.9	80.4	66.3	72.5	89.8
PC [51]	ECCV 2020	72.3	80.9	90.1	26.2	33.0	79.9	68.1	73.5	90.0
CSC [16]	CVPR 2021	72.8	81.0	90.7	26.9	33.7	80.6	70.7	76.4	90.8
MSC [46]	CVPR 2023	78.2	85.3	92.2	33.4	43.7	83.4	69.9	74.9	91.2
PTv3 [47]	CVPR 2024	77.6	85.0	92.0	35.3	46.0	83.4	73.4	78.9	91.7
HybridTM [44]	IROS 2025	77.8	-	-	36.5	-	-	72.1	-	-
CDSegNet [33]	CVPR 2025	77.9	85.2	92.2	36.3	45.9	83.9	-	-	-
Pamba [20]	AAAI 2025	77.6	-	-	36.3	-	-	73.5	-	-
DeepLA-120 [56]	CVPR 2025	77.6	-	-	-	-	-	75.7	-	-
PPT [48]	CVPR 2024	78.6	85.9	92.3	36.0	46.2	83.8	74.3	80.1	92.0
Sonata [49]	CVPR 2025	79.4	86.1	92.5	36.8	46.5	84.4	76.0	81.6	93.0
DoReMi (Ours)	-	80.1	87.3	93.1	37.2	47.9	84.4	77.2	82.5	93.1

The domain-aware branch dynamically modulates the sparsity and diversity of expert activation, ensuring stable and efficient expert allocation across diverse domains and operational scenarios, thereby enhancing the model's robustness and adaptability. The output feature is computed as:

$$f^o = f^{\text{Do}} + f^{\text{Re}}. (9)$$

3.5. Training Recipe

First, we obtain a pretrained model through multi-attribute self-supervised learning and use student model's weights to initialize the parameters of the DoReMi network. Subsequently, we implement multi-dataset joint training for segmentation as in PPT [48], which unifies cross-dataset category representation through a CLIP-head optimized via InfoNCE loss [25]. The overall training loss is as follows:

$$\mathcal{L}_{joint} = \mathcal{L}_{InfoNCE} + \lambda \mathcal{L}_{balance}. \tag{10}$$

After completing the joint training, the resulting model can be directly deployed for the primary tasks within the joint training framework and further fine-tuned to address diverse downstream tasks on novel datasets.

Taking semantic segmentation and multimodal detection as examples. The segmentation loss is defined as the standard cross-entropy loss:

$$\mathcal{L}_{\text{seg}} = -\frac{1}{M} \sum_{i=1}^{M} \sum_{c=1}^{C} y_{i,c} \log(q_{i,c}), \tag{11}$$

where M denotes the number of samples, C is the number of classes, $y_{i,c}$ represents the ground-truth label, and $q_{i,c}$ is the predicted probability for class c of sample i.

For the multi-modal detection task, we follow SpatialLM [23] and leverage the autoregressive property of the Qwen2.5 language model [42] to treat coordinate prediction as a sequence generation task. We adopt the same standard

cross-entropy loss as used in Qwen [42]:

$$\mathcal{L}_{\text{det}} = -\frac{1}{T} \sum_{t=1}^{T} \log P(w_t | w_{< t}, \theta),$$
 (12)

where T is the length of the coordinate sequence, w_t denotes the t-th coordinate element in the sequence, $w_{< t}$ represents the history of previously generated coordinates, and θ denotes the model parameters.

The overall fine-tune training objective is:

$$\mathcal{L}_{ft} = \mathcal{L}_{task} + \lambda \mathcal{L}_{balance}, \tag{13}$$

where \mathcal{L}_{task} denotes the task-specific loss (e.g., \mathcal{L}_{seg} for segmentation, \mathcal{L}_{det} for detection).

4. Experiments

4.1. Implementation Details

We conduct self-supervised learning on six mainstream datasets, including ScanNet [8], S3DIS [1], Structured3D [61], 3D-Front [12], ARKitScenes [2] and HM3D [53], comprising a total of 47,273 training samples. The network architecture follows the same design as Sonata, featuring 5 stages with block counts of 3, 3, 3, 12, and 3 per stage. Pretraining configurations are as follows: batch size is set to 64, learning rate is 0.0004, and training spans 50 epochs. Following Sonata [49], patch masking employs a cosine scheduler. Furthermore, density variations and color dropout are applied with different sampling ratios across patches. More experimental details are provided in supplementary materials. For the DoReMi architecture, the maximum expert number K is set to 8. λ is set to 0.001. The encoder architecture closely follows the pretrained network, with Re and Do branches added only to the final block of each stage. Domain embeddings are randomly initialized. All experiments are conducted on 8 NVIDIA A100 GPUs, with AdamW optimizer employed throughout.

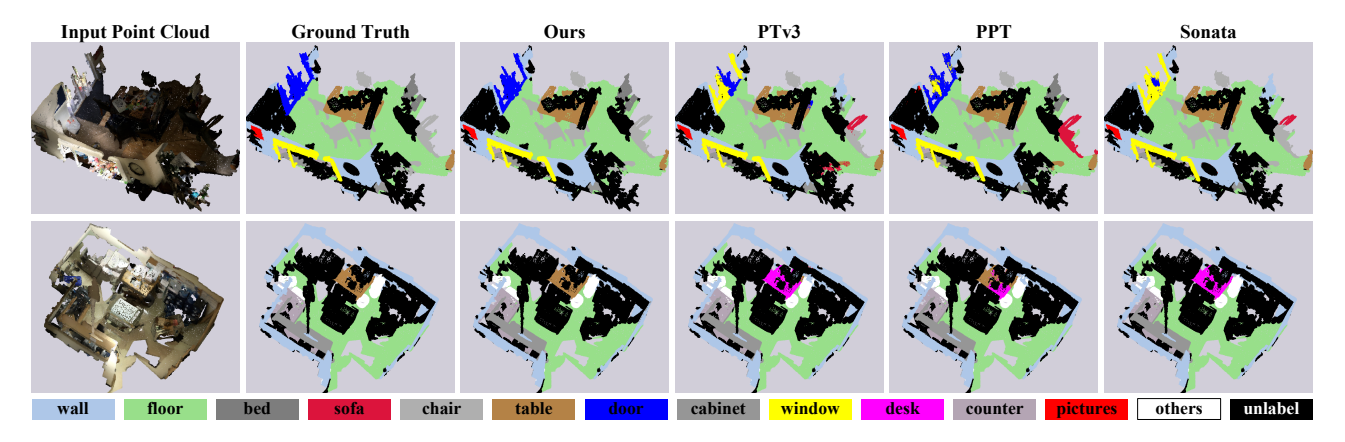


Figure 3. Qualitative analysis. Visualization of different methods on ScanNet.

Table 2. **Outdoor semantic segmentation.** * indicates results reproduced from the official repository.

Method	Nuscenes Val			Waymo Val		
Michiod	mIoU	mAcc	allAcc	mIoU	mAcc	allAcc
PTv3 [47]	80.4	87.2	94.7	71.3	80.5	94.7
Sonata* [49]	81.2	87.7	94.8	72.1	82.6	94.8
DoReMi (Ours)	81.7	87.4	94.8	72.7	82.7	94.8

4.2. Experimental Results

Indoor Semantic Segmentation. Following PPT [48], we conduct joint training on three datasets: ScanNet (20 classes), S3DIS (13 classes), and Structured3D (25 classes). To achieve cross-dataset semantic alignment of categories, we incorporate a CLIP-based classification head. We directly evaluated performance on ScanNet and S3DIS. Furthermore, we fine-tune our model on the more challenging ScanNet200 benchmark, achieving state-of-the-art performance across all three core metrics (mIoU, mAcc, and allAcc), as detailed in Table 1. Specifically, our method attains mIoU scores of 80.1%, 37.2%, and 77.2% respectively, representing improvements of 0.5%, 0.4%, and 1.2% over Sonata. Figure 3 presents a qualitative comparison with other methods. In the first scenario, when confronted with an incomplete chair, other approaches misidentify it as a sofa, whereas our method correctly recognizes it as a chair. This demonstrates that the Re obtained through SSL significantly enhances the model's capability to extract discriminative features from incomplete objects. In the second scenario, while other methods erroneously classify a table as a desk, our approach leverages DSR to integrate surrounding spatial context information. This enables precise routing of inputs to specialized expert networks through spatial feature analysis, thereby achieving superior recognition performance by fully exploiting contextual dependencies and domain-specific knowledge. These results demonstrate DoReMi's superior cross-domain adaptability and generalization capability in complex indoor scenarios.

Table 3. **Extension to unseen scenes.** Segmentation results on Matterport3D validation set.

Method	mIoU	mAcc	allAcc
PTv3 [47]	54.5	65.0	81.5
Sonata [49]	56.1	65.9	82.3
DoReMi (Ours)	57.1	68.2	83.3

Table 4. **Multimodal object detection** results on the ARK-itScenes validation set.

Method	F1@0.25	F1@0.5
SpatialLM [23] + Sonata [49]	58.9	49.5
SpatialLM [23] + DoReMi (Ours)	60.8	51.9

Outdoor Semantic Segmentation. Following indoor experimental setup, we conduct joint training and direct evaluation on nuScenes [3] and Waymo [40] datasets. As presented in Table 2, our model achieves mIoU scores of 81.7% and 72.7% on nuScenes and Waymo datasets respectively, representing 0.5% and 0.6% improvements over Sonata. These results validate DoReMi's superior generalization capability in outdoor scenarios.

Extension to Unseen Scenes. Beyond the observed performance on standard benchmarks, we demonstrate that the jointly trained model exhibits superior generalization capabilities in unseen scenarios. We evaluate this aspect by fine-tuning on the Matterport3D [5], which is a large-scale indoor RGB-D dataset containing 90 building-scale scenes. The domain embedding is obtained by averaging those from multiple datasets during joint training. As shown in Table 3, our model achieves 57.1% mIoU, 68.2% mAcc, and 83.3% allAcc on this unseen domain, outperforming Sonata by 1.0%, 2.3%, and 1.0%, respectively. These results substantiate the model's strong cross-scenario generalization ability, enabling effective knowledge transfer to adapt to diverse visual tasks and data distributions.

Multimodal Object Detection. Beyond segmentation, our method also extends effectively to detection tasks. In this

Table 5. Ablation study on each component.

Pa DSP FDA		ScanNet Val mIoU mAcc allAcc			S3DIS Val			
ΚC	DSK	LDA	mIoU	mAcc	allAcc	mIoU	mAcc	allAcc
×	×	×	77.5	85.4	92.1	73.5	78.9	92.0
\checkmark	×	×	78.8	85.9	92.5	75.7	81.4	92.5
\checkmark	\checkmark	×	79.5	87.0	92.9	76.4	82.1	93.0
\checkmark	\checkmark	\checkmark	80.1	87.3	92.1 92.5 92.9 93.1	77.2	82.5	93.1

Table 6. Comparison of DoReMi layer placement positions.

	N_{MoE}	mIoU	mAcc	allAcc
#1	3	79.4	86.8	92.7
#2	5	80.1	87.3	93.1
#3	10	79.9	87.2	92.9

experiment, we implement the SpatialLM [23] for object detection on the ARKitScenes dataset [2]. Evaluation employs F1-score metrics under two IoU thresholds (0.25 and 0.5). We establish the baseline using officially fine-tuned SpatialLM model weights with Sonata-based point cloud encoder, which serves as the initialization for DoReMi's subsequent fine-tuning. The optimization employs a learning rate of 0.00005 over 10 epochs. As summarized in Table 4, our method achieves 60.8% F1@0.25 and 51.9% F1@0.5, outperforming the baseline by 1.9% and 2.4%. These results validate the cross-task effectiveness of our framework and demonstrate its potential for extension to diverse vision tasks.

4.3. Ablation Studies

Component Ablation. As shown in Table 5, we conduct ablation studies on ScanNet and S3DIS to validate the effectiveness of each core component in DoReMi framework. First, when only Re branch is enabled, the model achieves improvements of 1.3% and 2.2% in mIoU compared to the baseline method PPT, demonstrating that Re branch enhances the model's ability to capture shared semantic patterns in multi-domain data through generic pretrained knowledge. Further incorporating DSR, with two experts selected, yields an additional 0.7% gain on both datasets. This improvement verifies that DSR can dynamically select the most relevant expert subsets based on the domain characteristics of input samples, thereby enhancing the model's adaptability and generalization capability in multi-domain scenarios. Finally, when EDA is integrated, the model achieves optimal performance with mIoU scores of 80.1% and 77.2%. EDA further improves expert utilization efficiency and training stability by optimizing expert load balancing and activation counts. These results demonstrate the effectiveness and synergy of DoReMi's modules: the Re branch enhances feature representation, DSR enables efficient domain-adaptive routing, and EDA ensures load balancing and dynamic optimization. Together, they form

Table 7. **Expert Number.** Evaluation of performance variations under different expert numbers in the Do branch.

Num	mIoU	mAcc	allAcc
4	79.6	87.2	92.8
6	79.7	86.9	93.0
8	80.1	87.3	93.1
10	79.5	87.1	92.9
12	79.4	86.6	92.7

Table 8. **Evaluation of expert load balancing performance.** We use the normalized standard deviation as the metric.

Method	$\alpha \downarrow$
Native MoE	0.941
DoReMi (Ours)	0.894

a robust, scalable framework for multi-domain point cloud understanding.

MoE-specific Analysis. We analyze the design of experts in DoReMi Layer and its load balancing. Table 6 shows the impact of inserting DoReMi layers at different encoder stages. Specifically, #1 inserts them at the final Block of stage 1, 3, and 5, totaling 3 insertion points; #2 inserts them at the final Block of every stage, totaling 5 insertion points; #3 inserts them at both the first and final Blocks of each stage, totaling 10 insertion points. Experimental results indicate that #2 achieves the best performance, reaching a performance metric of 80.1%. Insufficient insertion points (e.g., #1) limit the model's ability to adequately capture hierarchical feature representations, while excessive insertions (e.g., #3) may introduce redundancy. Table 7 analyzes the effect of the number of experts in the Do branch. Experiments show that using 8 experts yields the best performance. Fewer experts (e.g., 4) limit model expressiveness, while more experts increase complexity, training instability, and overfitting risk. Table 8 evaluates load balancing using the normalized standard deviation of expert activation counts, denoted as:

$$\alpha = \frac{\sqrt{\frac{1}{K} \sum_{j=1}^{K} (c_j - \bar{c})^2}}{\bar{c}},$$
(14)

where $\bar{c} = \frac{1}{K} \sum_{j=1}^{K} c_j$. In "Native MoE", 8 experts are configured with 2 experts fixed for activation, while our method employs EDA. Experimental results show that our method achieves a lower normalized standard deviation compared to "Native MoE", indicating that our mechanism distributes expert load more evenly, achieving superior load balancing performance and effectively improving computational efficiency and model stability.

Expert Activation Analysis. Figure 4 shows the activation frequency of Do branch experts in the second DoReMi layer across domains, with additional results in the supple-

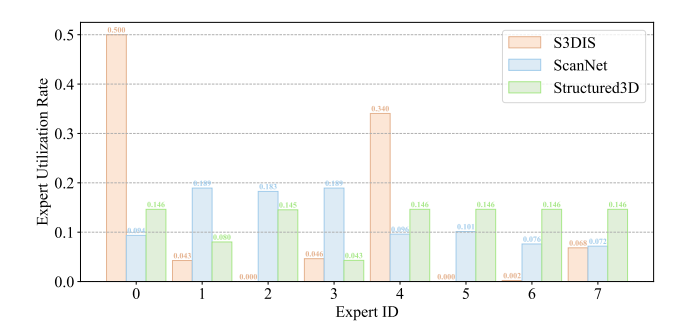


Figure 4. **Expert utilization rates across different datasets.** Taking Encoder Stage 2 as an example, y-axis values represent dataset-specific normalized utilization. More distribution results can be found in the supplementary materials.

mentary material. In S3DIS, Experts 0 and 4 are activated more frequently, suggesting they specialize to the dataset's spatial and semantic patterns. In Structured3D, activations are more balanced due to diverse scene types, allowing the model to leverage multiple experts for robust generalization. This demonstrates that dynamic routing enables experts to adaptively focus on domain-specific features in multi-domain scenarios.

Effectiveness of Pretraining Strategies. the adaptability and effectiveness of the DoReMi framework under different pretrained representations, we present in Table 9 the experimental results obtained by initializing the model with various pretraining strategies. The comparison between #1 and #2 demonstrates that, under identical pretrained weights, incorporating the structural design of DoReMi significantly improves model performance, indicating its ability to effectively integrate and enhance existing representations. The contrast between #2 and #3 shows that, when pretrained solely on point cloud modality, our multi-attribute self-supervised learning achieves better results, suggesting that richer pretraining signals enable DoReMi to better preserve cross-domain geometric and structural priors, thereby improving generalization. Recently, Concerto [59] introduced 2D-3D joint self-supervised learning, which leverages additional image modalities to obtain stronger representations. Combining its pretrained weights with the DoReMi architecture further pushes the state-of-the-art performance, demonstrating that DoReMi's structural design is compatible with various pretraining paradigms and can effectively enhance performance on top of strong feature representations.

Efficiency Comparison. We further analyze the efficiency–accuracy trade-off of DoReMi and previous methods. As shown in Table 10, Sonata [49] achieves higher performance than PPT [48] but at the cost of a large activated parameter increase. In contrast, our DoReMi further improves mIoU over Sonata (+0.7%) with only a moderate parameter growth. To verify that the performance gains are

Table 9. Comparison of different pretraining strategies.

	Method	Visual N	Modality 3D	mIoU	mAcc	allAcc
#1	Sonata [49]	×	√	79.4	86.1	92.5
	Sonata+Ours	×	√	79.7	87.0	92.8
#3	DoReMi (Ours)	×	✓	80.1	87.3	93.1
#4	Concerto [59]	✓	✓	80.7	87.4	93.1
#5	Concerto+Ours	✓	✓	81.2	89.1	93.2

Table 10. **Efficiency comparison.** ' and " represent Sonata variant. "Act. Params" indicates the number of activated parameters. FPS is measured on one A100 GPU.

	Method	Act. Params	FPS	mIoU
#1	PTv3 [47]	46.2M	11.0	77.6
#2	PPT [48]	46.3M	7.2	78.6
#3	Sonata [49]	124.8M	5.9	79.4
#4	Sonata'	147.6M	5.3	79.4
#5	Sonata"	148.6M	4.9	79.6
#6	DoReMi (Ours)	147.5M	4.9	80.1

not merely due to model scaling, we implement two larger variants of Sonata. The first sets the stage depths to [2, 2, 6, 2] and expands the channel dimensions to [64, 128, 256, 512], as shown in #4, while the second increases the depth of all four decoder stages to 5, as shown in #5. Both variants have a comparable number of parameters to DoReMi and follow the official implementation and training settings. Despite having similar model capacity, these variants still underperform compared to DoReMi, demonstrating that the observed improvements primarily stem from our domain–representation mixture design rather than parameter scaling. Overall, DoReMi delivers a superior accuracy–efficiency balance, converting limited additional computation into consistent improvements.

5. Conclusion

In this paper, we introduce DoReMi, a novel framework for generalizable 3D understanding, which jointly models domain-aware and general representations to reduce negative transfer in joint training across heterogeneous point cloud datasets. DoReMi consists of three key components. The Re branch, pretrained through robust multi-attribute self-supervised learning, preserves cross-domain geometric priors while maintaining global consistency. DSR selects domain-aware experts through context awareness, while EDA allocates the number of experts based on entropy, thereby adaptively modeling diverse domain distributions. Experiments on multiple downstream tasks show that DoReMi consistently outperforms existing methods in both accuracy and generalization.

References

- [1] Iro Armeni, Ozan Sener, Amir R Zamir, Helen Jiang, Ioannis Brilakis, Martin Fischer, and Silvio Savarese. 3d semantic parsing of large-scale indoor spaces. In *CVPR*, 2016. 5
- [2] Gilad Baruch, Zhuoyuan Chen, Afshin Dehghan, Tal Dimry, Yuri Feigin, Peter Fu, Thomas Gebauer, Brandon Joffe, Daniel Kurz, Arik Schwartz, et al. Arkitscenes: A diverse real-world dataset for 3d indoor scene understanding using mobile rgb-d data. arXiv preprint arXiv:2111.08897, 2021. 1, 5, 7
- [3] Holger Caesar, Varun Bankiti, Alex H Lang, Sourabh Vora, Venice Erin Liong, Qiang Xu, Anush Krishnan, Yu Pan, Giancarlo Baldan, and Oscar Beijbom. nuscenes: A multimodal dataset for autonomous driving. In CVPR, 2020. 6
- [4] Mathilde Caron, Ishan Misra, Julien Mairal, Priya Goyal, Piotr Bojanowski, and Armand Joulin. Unsupervised learning of visual features by contrasting cluster assignments. *NeurIPS*, 2020. 4
- [5] Angel Chang, Angela Dai, Thomas Funkhouser, Maciej Halber, Matthias Niessner, Manolis Savva, Shuran Song, Andy Zeng, and Yinda Zhang. Matterport3d: Learning from rgb-d data in indoor environments. arXiv preprint arXiv:1709.06158, 2017. 6
- [6] Sijin Chen, Xin Chen, Chi Zhang, Mingsheng Li, Gang Yu, Hao Fei, Hongyuan Zhu, Jiayuan Fan, and Tao Chen. Ll3da: Visual interactive instruction tuning for omni-3d understanding reasoning and planning. In CVPR, 2024. 1
- [7] Christopher Choy, Jun Young Gwak, and Silvio Savarese. 4d spatio-temporal convnets: Minkowski convolutional neural networks. In CVPR, 2019. 5
- [8] Angela Dai, Angel X Chang, Manolis Savva, Maciej Halber, Thomas Funkhouser, and Matthias Nießner. Scannet: Richly-annotated 3d reconstructions of indoor scenes. In CVPR, 2017. 1, 5
- [9] Jia Deng, Wei Dong, Richard Socher, Li-Jia Li, Kai Li, and Li Fei-Fei. Imagenet: A large-scale hierarchical image database. In CVPR, 2009. 1
- [10] Alexey Dosovitskiy. An image is worth 16x16 words: Transformers for image recognition at scale. arXiv preprint arXiv:2010.11929, 2020. 1
- [11] William Fedus, Barret Zoph, and Noam Shazeer. Switch transformers: Scaling to trillion parameter models with simple and efficient sparsity. *JMLR*, 2022. 2, 4
- [12] Huan Fu, Bowen Cai, Lin Gao, Ling-Xiao Zhang, Jiaming Wang, Cao Li, Qixun Zeng, Chengyue Sun, Rongfei Jia, Binqiang Zhao, et al. 3d-front: 3d furnished rooms with layouts and semantics. In *ICCV*, 2021. 5
- [13] Xumeng Han, Longhui Wei, Zhiyang Dou, Zipeng Wang, Chenhui Qiang, Xin He, Yingfei Sun, Zhenjun Han, and Qi Tian. Vimoe: An empirical study of designing vision mixture-of-experts. arXiv preprint arXiv:2410.15732, 2024.
- [14] Kaiming He, Xiangyu Zhang, Shaoqing Ren, and Jian Sun. Deep residual learning for image recognition. In CVPR, 2016.

- [15] Tong He, Wei Yin, Chunhua Shen, and Anton Van den Hengel. Pointinst3d: Segmenting 3d instances by points. In ECCV, 2022. 2
- [16] Ji Hou, Benjamin Graham, Matthias Nießner, and Saining Xie. Exploring data-efficient 3d scene understanding with contrastive scene contexts. In CVPR, 2021. 5
- [17] Robert A Jacobs, Michael I Jordan, Steven J Nowlan, and Geoffrey E Hinton. Adaptive mixtures of local experts. *Neu*ral Comput., 1991. 2
- [18] Li Jiang, Hengshuang Zhao, Shaoshuai Shi, Shu Liu, Chi-Wing Fu, and Jiaya Jia. Pointgroup: Dual-set point grouping for 3d instance segmentation. In CVPR, 2020. 2
- [19] Alex H Lang, Sourabh Vora, Holger Caesar, Lubing Zhou, Jiong Yang, and Oscar Beijbom. Pointpillars: Fast encoders for object detection from point clouds. In CVPR, pages 12697–12705, 2019. 2
- [20] Zhuoyuan Li, Yubo Ai, Jiahao Lu, ChuXin Wang, Jiacheng Deng, Hanzhi Chang, Yanzhe Liang, Wenfei Yang, Shifeng Zhang, and Tianzhu Zhang. Pamba: Enhancing global interaction in point clouds via state space model. In AAAI, 2025.
- [21] Isaak Lim, Moritz Ibing, and Leif Kobbelt. A convolutional decoder for point clouds using adaptive instance normalization. In Computer graphics forum, 2019. 1, 2
- [22] Yueen Ma, Yuzheng Zhuang, Jianye Hao, and Irwin King. 3d-moe: A mixture-of-experts multi-modal llm for 3d vision and pose diffusion via rectified flow. arXiv preprint arXiv:2501.16698, 2025. 2
- [23] Yongsen Mao, Junhao Zhong, Chuan Fang, Jia Zheng, Rui Tang, Hao Zhu, Ping Tan, and Zihan Zhou. Spatiallm: Training large language models for structured indoor modeling. In *NeurIPS*, 2025. 1, 5, 6, 7
- [24] Basil Mustafa, Carlos Riquelme, Joan Puigcerver, Rodolphe Jenatton, and Neil Houlsby. Multimodal contrastive learning with limoe: the language-image mixture of experts. *NeurIPS*, 2022. 2
- [25] Aaron van den Oord, Yazhe Li, and Oriol Vinyals. Representation learning with contrastive predictive coding. arXiv preprint arXiv:1807.03748, 2018. 5
- [26] Maxime Oquab, Timothée Darcet, Theo Moutakanni, Huy V. Vo, Marc Szafraniec, Vasil Khalidov, Pierre Fernandez, Daniel Haziza, Francisco Massa, Alaaeldin El-Nouby, Russell Howes, Po-Yao Huang, Hu Xu, Vasu Sharma, Shang-Wen Li, Wojciech Galuba, Mike Rabbat, Mido Assran, Nicolas Ballas, Gabriel Synnaeve, Ishan Misra, Herve Jegou, Julien Mairal, Patrick Labatut, Armand Joulin, and Piotr Bojanowski. Dinov2: Learning robust visual features without supervision, 2023. 3
- [27] Yatian Pang, Wenxiao Wang, Francis EH Tay, Wei Liu, Yonghong Tian, and Li Yuan. Masked autoencoders for point cloud self-supervised learning. In *ECCV*, 2022. 2
- [28] Songyou Peng, Kyle Genova, Chiyu Jiang, Andrea Tagliasacchi, Marc Pollefeys, Thomas Funkhouser, et al. Openscene: 3d scene understanding with open vocabularies. In CVPR, 2023. 2
- [29] Charles R Qi, Hao Su, Kaichun Mo, and Leonidas J Guibas. Pointnet: Deep learning on point sets for 3d classification and segmentation. In CVPR, 2017. 2

- [30] Charles Ruizhongtai Qi, Li Yi, Hao Su, and Leonidas J Guibas. Pointnet++: Deep hierarchical feature learning on point sets in a metric space. *NeurIPS*, 2017. 2
- [31] Guocheng Qian, Yuchen Li, Houwen Peng, Jinjie Mai, Hasan Hammoud, Mohamed Elhoseiny, and Bernard Ghanem. Pointnext: Revisiting pointnet++ with improved training and scaling strategies. *NeurIPS*, 2022. 2
- [32] Can Qin, Haoxuan You, Lichen Wang, C-C Jay Kuo, and Yun Fu. Pointdan: A multi-scale 3d domain adaption network for point cloud representation. *NeurIPS*, 2019. 1, 2
- [33] Wentao Qu, Jing Wang, YongShun Gong, Xiaoshui Huang, and Liang Xiao. An end-to-end robust point cloud semantic segmentation network with single-step conditional diffusion models. In CVPR, 2025. 5
- [34] Samyam Rajbhandari, Conglong Li, Zhewei Yao, Minjia Zhang, Reza Yazdani Aminabadi, Ammar Ahmad Awan, Jeff Rasley, and Yuxiong He. Deepspeed-moe: Advancing mixture-of-experts inference and training to power next-generation ai scale. In *ICML*, pages 18332–18346, 2022. 2
- [35] Carlos Riquelme, Joan Puigcerver, Basil Mustafa, Maxim Neumann, Rodolphe Jenatton, André Susano Pinto, Daniel Keysers, and Neil Houlsby. Scaling vision with sparse mixture of experts. *NeurIPS*, 2021. 2
- [36] Alexandre Sablayrolles, Matthijs Douze, Cordelia Schmid, and Hervé Jégou. Spreading vectors for similarity search. arXiv preprint arXiv:1806.03198, 2018. 4
- [37] Christoph Schuhmann, Romain Beaumont, Richard Vencu, Cade Gordon, Ross Wightman, Mehdi Cherti, Theo Coombes, Aarush Katta, Clayton Mullis, Mitchell Wortsman, et al. Laion-5b: An open large-scale dataset for training next generation image-text models. *NeurIPS*, 2022. 1
- [38] Shuai Shao, Zeming Li, Tianyuan Zhang, Chao Peng, Gang Yu, Xiangyu Zhang, Jing Li, and Jian Sun. Objects365: A large-scale, high-quality dataset for object detection. In *ICCV*, 2019. 1
- [39] Shaoshuai Shi, Chaoxu Guo, Li Jiang, Zhe Wang, Jianping Shi, Xiaogang Wang, and Hongsheng Li. Pv-rcnn: Pointvoxel feature set abstraction for 3d object detection. In CVPR, 2020. 2
- [40] Pei Sun, Henrik Kretzschmar, Xerxes Dotiwalla, Aurelien Chouard, Vijaysai Patnaik, Paul Tsui, James Guo, Yin Zhou, Yuning Chai, Benjamin Caine, et al. Scalability in perception for autonomous driving: Waymo open dataset. In CVPR, 2020. 6
- [41] Antti Tarvainen and Harri Valpola. Mean teachers are better role models: Weight-averaged consistency targets improve semi-supervised deep learning results. *NeurIPS*, 2017. 3
- [42] Qwen Team et al. Qwen2 technical report. arXiv preprint arXiv:2407.10671, 2024. 5
- [43] Hugues Thomas, Charles R Qi, Jean-Emmanuel Deschaud, Beatriz Marcotegui, François Goulette, and Leonidas J Guibas. Kpconv: Flexible and deformable convolution for point clouds. In *ICCV*, 2019. 2
- [44] Xinyu Wang, Jinghua Hou, Zhe Liu, and Yingying Zhu. Hybridtm: Combining transformer and mamba for 3d semantic segmentation. In *IROS*, 2025. 5

- [45] Xiaoyang Wu, Yixing Lao, Li Jiang, Xihui Liu, and Hengshuang Zhao. Point transformer v2: Grouped vector attention and partition-based pooling. *NeurIPS*, 2022. 2
- [46] Xiaoyang Wu, Xin Wen, Xihui Liu, and Hengshuang Zhao. Masked scene contrast: A scalable framework for unsupervised 3d representation learning. In CVPR, 2023. 5
- [47] Xiaoyang Wu, Li Jiang, Peng-Shuai Wang, Zhijian Liu, Xi-hui Liu, Yu Qiao, Wanli Ouyang, Tong He, and Hengshuang Zhao. Point transformer v3: Simpler faster stronger. In CVPR, 2024. 2, 5, 6, 8
- [48] Xiaoyang Wu, Zhuotao Tian, Xin Wen, Bohao Peng, Xihui Liu, Kaicheng Yu, and Hengshuang Zhao. Towards largescale 3d representation learning with multi-dataset point prompt training. In CVPR, 2024. 1, 5, 6, 8
- [49] Xiaoyang Wu, Daniel DeTone, Duncan Frost, Tianwei Shen, Chris Xie, Nan Yang, Jakob Engel, Richard Newcombe, Hengshuang Zhao, and Julian Straub. Sonata: Selfsupervised learning of reliable point representations. In CVPR, 2025. 2, 3, 5, 6, 8
- [50] Chunlong Xia, Xinliang Wang, Feng Lv, Xin Hao, and Yifeng Shi. Vit-comer: Vision transformer with convolutional multi-scale feature interaction for dense predictions. In CVPR, 2024. 1
- [51] Saining Xie, Jiatao Gu, Demi Guo, Charles R Qi, Leonidas Guibas, and Or Litany. Pointcontrast: Unsupervised pretraining for 3d point cloud understanding. In ECCV, 2020. 2, 5
- [52] Le Xue, Mingfei Gao, Chen Xing, Roberto Martín-Martín, Jiajun Wu, Caiming Xiong, Ran Xu, Juan Carlos Niebles, and Silvio Savarese. Ulip: Learning a unified representation of language, images, and point clouds for 3d understanding. In CVPR, 2023. 2
- [53] Karmesh Yadav, Ram Ramrakhya, Santhosh Kumar Ramakrishnan, Theo Gervet, John Turner, Aaron Gokaslan, Noah Maestre, Angel Xuan Chang, Dhruv Batra, Manolis Savva, et al. Habitat-matterport 3d semantics dataset. In CVPR, 2023. 5
- [54] Fan Yang, Hui Chen, Yuwei He, Sicheng Zhao, Chenghao Zhang, Kai Ni, and Guiguang Ding. Geometry-guided domain generalization for monocular 3d object detection. In AAAI, 2024. 1, 2
- [55] Jianing Yang, Xuweiyi Chen, Nikhil Madaan, Madhavan Iyengar, Shengyi Qian, David F Fouhey, and Joyce Chai. 3d-grand: A million-scale dataset for 3d-llms with better grounding and less hallucination. In CVPR, 2025. 1
- [56] Ziyin Zeng, Mingyue Dong, Jian Zhou, Huan Qiu, Zhen Dong, Man Luo, and Bijun Li. Deepla-net: Very deep local aggregation networks for point cloud analysis. In CVPR, 2025. 5
- [57] Renrui Zhang, Ziyu Guo, Peng Gao, Rongyao Fang, Bin Zhao, Dong Wang, Yu Qiao, and Hongsheng Li. Point-m2ae: multi-scale masked autoencoders for hierarchical point cloud pre-training. *NeurIPS*, 2022. 2
- [58] Yue Zhang, Yingzhao Jian, Hehe Fan, Yi Yang, and Roger Zimmermann. Uni3d-moe: Scalable multimodal 3d scene understanding via mixture of experts. *arXiv preprint arXiv:2505.21079*, 2025. 2

- [59] Yujia Zhang, Xiaoyang Wu, Yixing Lao, Chengyao Wang, Zhuotao Tian, Naiyan Wang, and Hengshuang Zhao. Concerto: Joint 2d-3d self-supervised learning emerges spatial representations. In *NeurIPS*, 2025. 8
- [60] Hengshuang Zhao, Li Jiang, Jiaya Jia, Philip HS Torr, and Vladlen Koltun. Point transformer. In *ICCV*, 2021. 1
- [61] Jia Zheng, Junfei Zhang, Jing Li, Rui Tang, Shenghua Gao, and Zihan Zhou. Structured3d: A large photo-realistic dataset for structured 3d modeling. In *ECCV*, 2020. 5
- [62] Junsheng Zhou, Jinsheng Wang, Baorui Ma, Yu-Shen Liu, Tiejun Huang, and Xinlong Wang. Uni3d: Exploring unified 3d representation at scale. *arXiv preprint arXiv:2310.06773*, 2023. 2
- [63] Yin Zhou and Oncel Tuzel. Voxelnet: End-to-end learning for point cloud based 3d object detection. In *CVPR*, 2018. 2